The mineralization of osteonal cement line depends on where the osteon is formed

Astrid Cantamessa [1*], Stéphane Blouin [2], Maximilian Rummler [3], Andrea Berzlanovich [4], Richard Weinkamer [3*], Markus A. Hartmann [2], Davide Ruffoni [1*]

[1] Mechanics of Biological and Bioinspired Materials Laboratory, Department of Aerospace and Mechanical Engineering, University of Liège, Liège, Belgium.

[2] Ludwig Boltzmann Institute of Osteology at Hanusch Hospital of OEGK and AUVA Trauma Centre Meidling, 1st Medical Department Hanusch Hospital, Vienna, Austria.

[3] Department of Biomaterials, Max Planck Institute of Colloids and Interfaces, Potsdam, Germany.

[4] Center of Forensics Medicine, Vienna, Austria.

* Corresponding authors

Astrid Cantamessa
Astrid.Cantamessa@uliege.be
University of Liege
Quartier Polytech 1
Allée de la Découverte 9
4000 Liège, Belgium

Davide Ruffoni
druffoni@uliege.be
University of Liege
Quartier Polytech 1
Allée de la Découverte 9
4000 Liège, Belgium

Richard Weinkamer
richard.weinkamer@mpikg.mpg.de
Max Planck Institute of Colloids and Interfaces, Science Park
Golm, 14424 Potsdam, Germany

Word count: 5438

Reference count: 47

Table/Figure count: 6

Abstract word count: 300

Keywords (5-10 keywords): cement line, mineralization, osteon, human bone, quantitative backscattered electron imaging, mineralization process, mineral content, mineral recycling, tissue age

Abstract

The cement line (CL) is a thin layer, 1-3 μm in width, separating secondary osteons from interstitial bone and other osteons. Despite the possible role for bone quality, the CL is still one of the least understood features of bone. This study aims to investigate how the mineral content of the CL varies not only with osteon age but also with the surrounding environment. Using quantitative backscattered electron imaging to measure the mineral content, we analyzed 35 osteons from femoral bone of two male individuals (40 and 81 years old). We implemented a new approach to investigate the mineral content based on a spatially resolved analysis in layers along the CL and incorporating regions both inside the osteon (formed soon after CL deposition) and outside (already present at the time of CL deposition). We found that the CLs had always higher mineral content than the corresponding osteon ($p < 0.001$), and that not only the osteon, but also the CL increases its mineral content with time. Including areas outside the osteon in the analysis improved considerable our understanding of CL mineralization. After a rapid primary phase where the CL incorporates more mineral than the osteon, secondary mineralization is about 60% slower in the CL than in the osteon. One key finding is that the mineralization of the CL is not universal but depends on the region in which the osteon is formed. This is supported by a strong correlation between the mineral content of the CL and outside the osteon ($R = 0.75$, $p < 0.001$), but not inside. One possible explanation is that mineral released during bone resorption may contribute to the mineralization of the cement line, as higher mineral content in resorbed bone was associated with greater mineralization in the cement line.

Lay summary

Bone is a dynamic tissue that self-renews through remodeling and mineralization. This leads to the formation of secondary osteons, tubular structures surrounded by a thin layer called cement line. This study explores the mineralization of the cement line. By examining osteons of different age in human femoral bone, we found that the mineral content in a newly deposited cement line is higher than in the corresponding osteon and that the mineralization of the cement line is not universal but depends on the surrounding in which it is formed.

Introduction

Cement lines (CLs) are thin interphases, typically 1-3 µm in width, which are ubiquitous in bone. They are found at: i) the border of secondary osteons in cortical bone[1], ii) around individual bone packets in trabecular bone[2] and iii) between bone and mineralized cartilage at entheses[3,4] and osteochondral junctions[4]. Despite their small thickness, CLs are assumed to contribute to bone fracture resistance by deflecting or arresting microcracks. In cortical bone, studies have shown that microcracks coming from the interstitial tissue, can deviate when meeting the CL[5–8]. Such a mechanism allows to dissipate energy, to reduce the force driving crack propagation[9], and also to preserve the overall integrity of the osteon. Indeed, microcracks are more likely observed in interstitial bone than inside osteons[10].

The ability of the CL to interact with damage depends on its basic mechanical properties such as stiffness, strength and toughness[11]. However, these properties are still not well characterized: there are only very limited data on CL stiffness and strength[12] and, to our knowledge, no data on fracture toughness. CL mineral content is one factor of fundamental importance for the mechanical behavior. Yet, the composition of CLs remains controversial: both lower[13] and higher[14] mineral content of CLs compared to surrounding bone are reported. More recent data indicate that CLs tend to have higher mineral content than the corresponding osteons[10,15,16], with the difference decreasing with tissue age[16]. Complementary Raman analysis has suggested that the higher degree of mineralization of the CL is combined with lower collagen content[16]. At the same time, the dimensions of the osteon do not seem to influence the degree of mineralization of the CL[16].

The mineral content of the osteon is not static but evolves in time according to a specific mineralization process. Current understanding is that a fast primary mineralization, bringing the mineral content up to about 70% of the final value within a few days, is followed by a much slower secondary mineralization. The latter leads to a gradual maturation of the mineral phase, which takes up to several years[17–20]. Conversely, knowledge about how much mineral is

incorporated during CL formation, and to which extent the mineral content of the CL evolves with time is insufficient.

CLs are found around secondary osteons, which are a result of cortical bone remodeling[21], with CLs providing a proper “cleaned” surface for osteoid deposition[1,22,23]. CLs have higher content of osteopontin (a CL marker) than adjacent bone[23]. The examination of cutting cones in osteons with serial sectioning has provided clues that in bone remodeling both osteoclasts and osteoprogenitor cells are able to form CLs during or immediately after bone resorption[1]. In bone modeling, however, CLs are laid down on surfaces not previously eroded, and only osteoprogenitors cells should be contributing to their formation.

A further element that can impact tissue mineralization is the transport of mineral ions to the mineralization site. There is evidence that locations of bone modeling and remodeling present differences in the mineralization process, resulting in specific mineral characteristics such as crystal composition and dimensions[24]. This is likely due to different avenues to transport ionic precursors. Usually bone modeling requires transport over large distances and, thus, ionic precursors should be stabilized by compositional modifications, whereas in bone remodeling this is not necessary as resorbed mineral may be locally recycled[24]. As the formation of CL and osteonal bone are somewhat dephased, both in space and time, differences in available mineral ions may be present, impacting the mineralization process.

The aim of this work is to characterize how the mineral content of CLs varies with the surrounding environment and changes over time. By examining osteons of different mineral content, potentially reflecting differences in tissue age, new insights into CL mineral content and mineralization can be obtained.

Materials and Methods

Sample preparation

Human femurs from two male donors including a 40-year old individual (height 175 cm, weight 77 kg, cause of death myocardial infarction) and a 81-year old individual (height 175 cm, weight 79 kg, cause of death myocardial infarction) without known metabolic bone disease were obtained from the Department of Forensic Medicine of the Medical University of Vienna, in accordance with the ethical commission of the institution (EK no. 1757/2013). After extraction, the bones were kept frozen at -20 °C until further preparation. Cross sections (perpendicular to the longitudinal axis of the femurs) of about 1.5 cm in thickness were cut from the femoral shaft far from the metaphysis (Figs. 1A and B) using a water-cooled diamond saw (Buehler Isomet 1000, Germany). The sections were then prepared following a well-established

procedure[25,26], which involved dehydration in graded ethanol series, followed by immersion in ethanol/acetone baths, and embedding in poly-methyl methacrylate (PMMA). The transverse surfaces were ground with sandpapers having decreasing grit size (P1200, P2400) and polished using a diamond suspension down to 1 µm particle size on a silk cloth under glycol irrigation (Logitech PM5, UK), to minimize the formation of microcracks[27].

Quantitative backscattered electron imaging (qBEI)

The local mineral content of cortical bone was quantified with qBEI, a well-established technique based on scanning electron microscopy (SEM), providing quantitative two-dimensional spatial maps of calcium content by measuring the intensity of the backscattered signal[26,28]. To obtain a conducting surface, a thin carbon layer was deposited on the polished samples by vacuum evaporation (Agar SEM carbon coater, Agar, Stansted, UK). The SEM, equipped with a zirconium-coated field emission cathode (Zeiss SEM SUPRA 40, Germany), was operated at 20 kV with a working distance of 10 mm, and a probe current of 280 – 320 pA. First, overview scans (Fig. 1C) with a larger field of view and a lower resolution (1.76 µm/pixel) were performed to select the osteons of interest for subsequent higher resolution analysis. The selected osteons had to feature a central Haversian canal and a continuous border i.e., they should not be interrupted by more recent osteons. In the analysis, we included osteons with different sizes and mineral contents, which is assumed as a proxy of tissue age. The chosen osteons (n = 35, 15 coming from the younger donor and 20 from the older one) and the surrounding bone were measured at higher magnification (pixel resolution 0.57 µm with a field of view of 1024 x 768 pixels). This resolution is high enough to resolve the CLs, which have a thickness in transverse sections of about 1-3 µm and low enough to allow for a quantitative measurement of the calcium content without additional contrast due to, e.g., orientation of bone lamellae. A calibration of the SEM backscattered signal with carbon and aluminum standards was performed as previously reported[26,29], to establish a quantitative relation between the measured grey level and the local mineral content, expressed as calcium weight percent (Ca wt %).

Second harmonic generation imaging

Second harmonic generation (SHG) imaging was performed at the same locations analyzed with qBEI to ensure that the selected osteons are the most recently deposited in their neighborhood. This can be challenging when two osteons with similar mineral content slightly overlap (Fig. 1D). By inspecting the lamellar organization accessible with SHG (Figs. 1F, G and S1), we look for osteons with uninterrupted lamellae, which is a clear indication of being the most recent ones. Samples were imaged using confocal laser scanning microscopy (Leica TCS SP8 DLS, Germany) with a 40x oil immersion objective (HC PL APO 40×/1.30 OIL). A

pulsed infrared laser (Spectra-Physics, Milpitas) at a wavelength of 910 nm was used, and the backward direction signal was detected at 450–460 nm wavelength. Images were acquired with a nominal pixel size of 379 nm and a field of view of 1024 x 1024 pixels at a scan rate of 400 Hz. Several neighboring regions were measured with a slight overlapping, ensuring proper alignment when stitching them together using the software of the Leica microscope. For an appropriate detection of lamellar arrangement, the SHG resolution was chosen to be smaller than typical lamellar thickness (~4 - 6 µm).

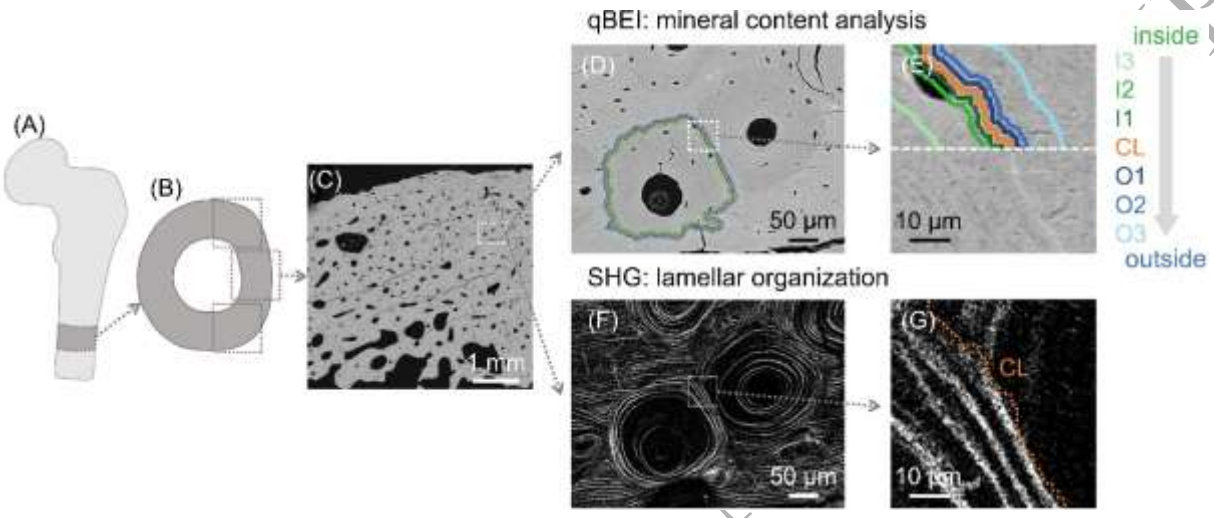

Fig. 1: Analysis of human osteonal bone. (A) Schematic of a human femur and (B) transverse cross-section where (C) qBEI scans were performed to select the osteons to be analyzed. (D) High resolution qBEI map of an uninterrupted osteon neighboring other osteons (top and bottom) and interstitial bone (left and right). (E) Magnified view of a CL and the different layers around the CL, located both inside (I1, I2, I3) and outside (O1, O2, O3) the selected osteon. (F) SHG image of the same region highlighting the uninterrupted lamellar organization of the selected osteon. (G) Close-up of the SHG image with the orange dashed line representing the location of the CL, detected by superimposing SHG and qBEI maps.

Mineral content of the cement line and adjacent regions: layers analysis

Before evaluating the mineral content, a 2-pixel erosion was applied to minimize boundary effects[17] using the software CTAn (v1.19.4.0, Skyscan). Background pixels, including osteocytes lacunae, Haversian canals and microcracks, were removed by discarding all pixels with a calcium content below 5.2 wt %. This ensured that only mineralized bone regions and no voids were included in the analysis. The mineral content of the CL and of neighboring bone was evaluated according to the following layer analysis, implemented in CTAn. First, a mask of each osteon (not including the CL) was generated by manually contouring the osteon border as delimited by the CL (Figs. S2A and B). This choice is motivated by the fact that the boundary between the CL and the osteon was usually easier to detect than between the CL and the interstitial bone. The manual contouring process was performed by a single operator to

maintain consistency, and the results were visually inspected by a second operator. The extracted mask was dilated with a round kernel of 2 pixels to include the CL, and the original mask of the osteon was subtracted from the dilated mask to obtain a 2-pixel (or 1.14 μm) thick circular layer representing the CL. Next, the bone around the CL was subdivided into several concentric circular layers having the same nominal thickness of the CL and located both inside and outside the osteon, in regions adjacent to the CL as well as further away (Figs. 1D and E). The layers were obtained by multiple cycles of erosion and dilation applied to the mask of the osteon (Figs. S2C and D). Specifically, we considered layers close to the CL and placed at 1 and 4 pixels (or 0.57 μm and 2.28 μm) away from the CL border: 2 layers inside the osteon (I1, I2) and 2 layers outside (O1, O2). Two additional layers were defined 20 pixels (or 11.4 μm) away from the CL (I3 and O3, respectively). Inner layers include only osteonal bone, whereas outer layers may intersect with other (older) osteons and interstitial bone. Furthermore, all concentric circular layers were radially sliced into 16 sectors (using MATLAB 2022a), which served to investigate the spatial variation of mineral content around the osteons (Fig. S2E). A custom MATLAB routine was implemented to compute the mean calcium content (Ca_{Mean}), its standard deviation, as well as the frequency distribution of the calcium content, within each layer and in the whole osteon. Considering the limited number of pixels in the layers, to improve readability of the plots, all frequency distributions were slightly smoothed with a running average filter (window size 10).

Statistical Analysis

We compared differences in mineralization among the layers by performing a Friedman test, chosen due to the non-normal distribution of the paired data. When significant differences were detected, pairwise comparisons between layers were conducted using post-hoc tests with Bonferroni correction to control for multiple comparisons and minimize false positive. We examined the strength of the relationships between the mean calcium content of osteon, CL and different layers using Spearman's rank correlation, selected for its suitability with non-normal distribution of the data. Significance levels were set at $p < 0.05$, and all p-values were two-sided. All statistical analyses were performed in MATLAB 2022a.

Results

From a qualitative observation of the qBEI maps, the CL appears as a thin line around the osteon (Fig. 1E). In the SHG images there were no evident features allowing a clear discrimination between CL and adjacent lamellar bone (Fig. 1G). However, superimposing qBEI and SHG maps indicates that the CL tends to fall in regions with no (or very weak) SHG signal.

We explore possible links between the mineralization of the CL and immediately adjacent bone, considering regions both outside and inside the osteon, i.e. formed before and after CL deposition, respectively. We first report detailed findings on two osteons having low and high mean mineral content that are representative for younger and older tissue (assuming mineral content as an indirect measure of tissue age) and extracted from the adult (40 years old) and aged (81 years old) individual, respectively. We then present results of all 35 osteons, with mean calcium content ranging from 21.37 ± 2.26 wt % to 26.43 ± 2.2 wt %, and therefore covering a large spectrum of tissue age. Less mineralized younger osteons were more likely found in the adult individual, whereas older more mineralized osteons were found in the aged individual.

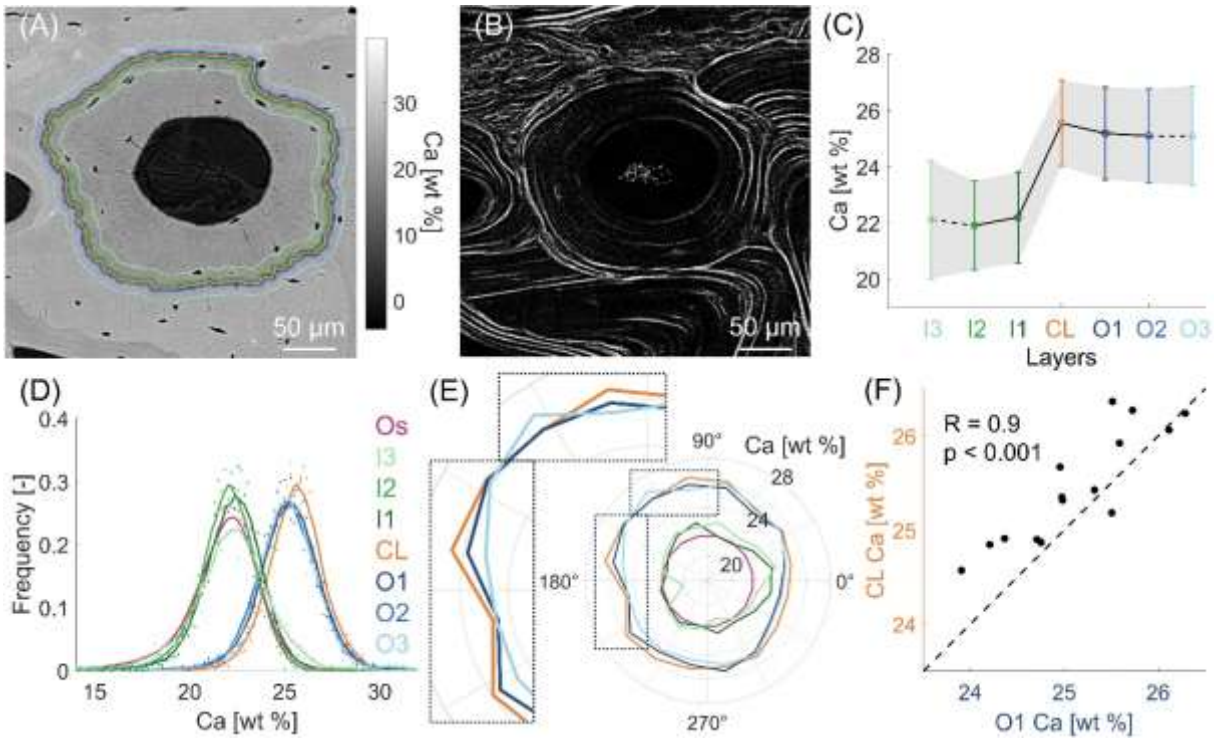

Fig. 2: Mineral content analysis of a lowly mineralized osteon from the adult (40 years) individual. (A) qBEI map with CL and layers highlighted by the colored lines. (B) SHG image showing the lamellar organization. (C) Mean calcium content of the inner layers (I3, I2, I1), CL and outer layers (O1, O2, O3). Data shown as mean ± standard deviation (the shaded area delimits a one-standard deviation interval around the mean). Data points are connected by lines to visualize the trend: full lines connect points equally spaced, whereas dashed lines indicate that I3 and O3 are further away. (D) Frequency distributions of the calcium content of the entire osteon (Os), CL and layers. Original data represented as scattered points and smoothed data (with moving average) as full lines. (E) Polar plot of the

calcium content in selected regions (CL, O1, O3, I1, I3 and Os), averaged over 16 sectors around the osteon. The mean Ca content in each sector is plotted as distance from the center. (F) Correlation between the calcium content of CL and O1 considering all 16 sectors. The dotted line with a unit slope and passing through the origin is shown to improve the readability of the plot.

As a first example, we investigated an osteon with relatively low mean mineral content (Ca_{Mean} = 21.72 ± 2.09 wt %) coming from the adult individual and surrounded by older osteons and interstitial bone (Fig. 2A). SHG imaging reveals bone lamellae at the osteon periphery, confirming that the selected osteon is not interrupted by other osteons (Fig. 2B). The local and layer-based analysis of qBEI map indicates a clear increase in mineral content of about 15% when going from the inner layers of the osteon to the CL, which has Ca_{Mean} of 25.54 ± 1.52 wt % (Fig. 2C). The difference in mineral content between the CL and the outer layers is much smaller (around 2%) but still statistically significant ($p < 0.001$). The same trend is confirmed when inspecting the frequency distributions of the calcium content of the layers, which essentially split into two groups (Fig. 2D): inner layers have similar distributions, overlapping with the distribution of the whole osteon, whereas the distributions of the outer layers are shifted towards higher mineral content. The frequency distribution of the CL displays an additional (albeit small) right-shift, making it distinguishable from all other curves. Owing to the circular shape of the osteon, the spatial correlation among the layers is further explored with a polar plot (Fig. 2E), based on the subdivision into 16 sectors (see Materials and Methods). In the polar plot, the mean calcium content in each sector is plotted as distance from the center. If two layers have similar calcium content in the same sector, the corresponding polar plots overlap. A central observation is that in each sector around the osteon, the mean calcium content of the CL follows very closely the mineral content of immediately adjacent bone located just outside the osteon and therefore deposited potentially long before the CL. The polar plot also gives an idea of how the spatial correlation varies across the 16 sectors: for example, when the osteon is close to interstitial bone with higher mineral content (top region of the plot), the mineral content of both the CL and the outer layer O1 slightly increases. An additional quantification is obtained by computing the Spearman correlation coefficient between the calcium content of the CL and of the adjacent outer layer O1 in the 16 sectors around osteon (Fig. 2F): with $R = 0.9$ ($p < 0.001$), such correlation can be considered as very strong[30]. Conversely, no spatial relationship between the mean mineral content of CL and inner layers is evident: the correlation between the calcium content of the CL and of the inner layer I1 in the 16 sectors is not statistically significant (Fig. S3A, $R = -0.4$, $p = 0.108$).

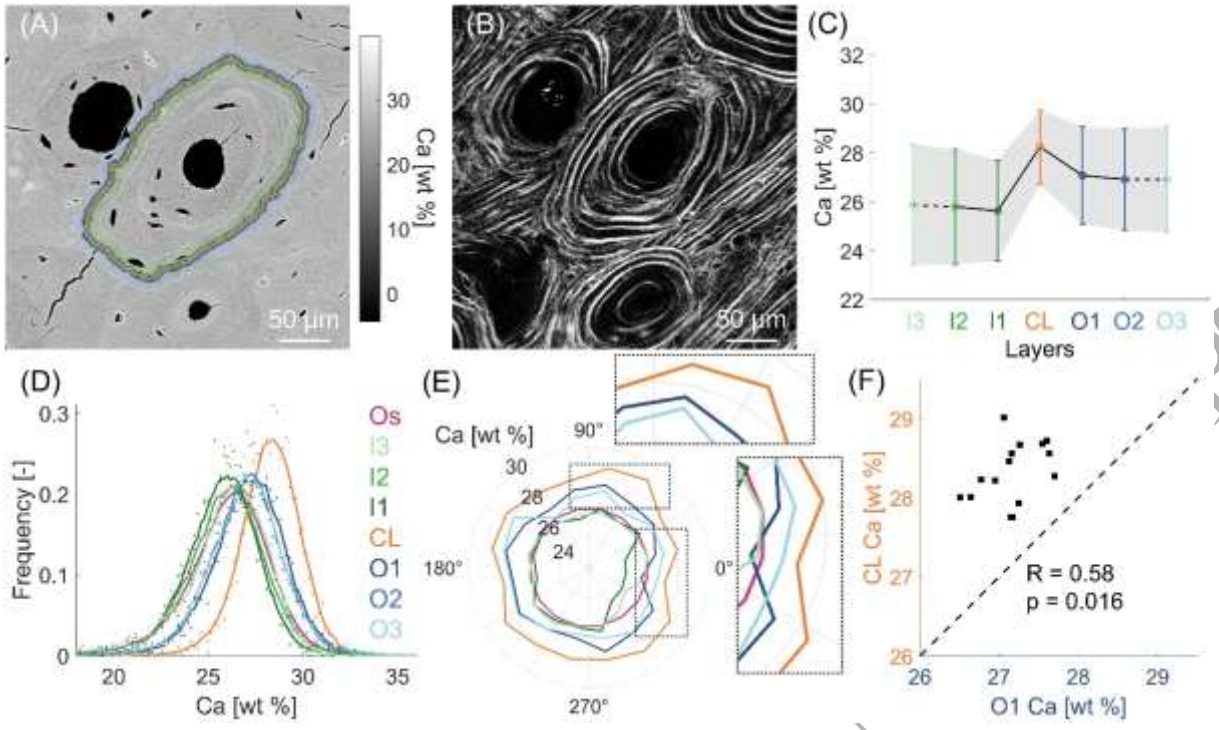

Fig. 3: Mineral content analysis of a highly mineralized osteon from the aged (81 years) individual. (A) qBEI map with CL and layers highlighted by the colored lines. (B) SHG image showing the lamellar organization. (C) Mean calcium content of the inner layers (I3, I2, I1), CL and outer layers (O1, O2, O3). Data shown as mean ± standard deviation (the shaded area delimits a one-standard deviation interval around the mean). Data points are connected by lines to visualize the trend: full lines connect points equally spaced, whereas dashed lines indicate that I3 and O3 are further away. (D) Frequency distributions of the calcium content of the entire osteon (Os), CL and layers. (E) Polar plot of the calcium content in selected regions (CL, O1, O3, I1, I3 and Os), averaged over 16 sectors around the osteon. The mean Ca content in each sector is plotted as distance from the center. (F) Correlation between the calcium content of CL and O1 considering all 16 discrete sectors. The dotted line with a slope of one and passing through the origin is shown to improve the readability of the plot.

The second example is an osteon with higher mineral content (Ca_{Mean} = 25.95 ± 2.45 wt %) representative for older tissue and extracted from the aged individual. Again, this osteon is surrounded by a heterogeneous environment featuring older osteons as well as interstitial bone (Fig. 3A and B). The SHG analysis underlines a clear pattern of alternating and uninterrupted bone lamellae within the selected osteon (Fig. 3B). In this “aged” scenario, the CL has still higher mineral content than the osteon (about 9%) as well as than the external surrounding bone layers (about 5%, Fig. 3C). The frequency distributions of inner and outer layers are closer to each other with respect to the previous case of the younger osteon, whereas the distribution of the CL still displays a noticeable shift to higher mineral content (Fig. 3D). The polar plot suggests a statistically significant spatial relationship between the mineral content of CL and adjacent outer layers (Fig. 3E), which is characterized by a moderate correlation coefficient ($R = 0.58$, $p < 0.05$). Also in this example, the correlation between the CL and the inner layer I1 is not significant (Fig. S3B, $R = 0.41$, $p = 0.101$).

Extending the layer analysis to all osteons (Fig. 4), confirms that the CLs always exhibit the highest mean mineral content (27.35 ± 1.58 wt % Ca), not only in comparison with the layers inside the osteons but also with the layers outside, apart from O1. The difference in mineral content between the CL and the outer layers is less pronounced than between the CL and the inner layers. The outer layers show a smaller spreading in the mean mineral content when compared to the inner layers.

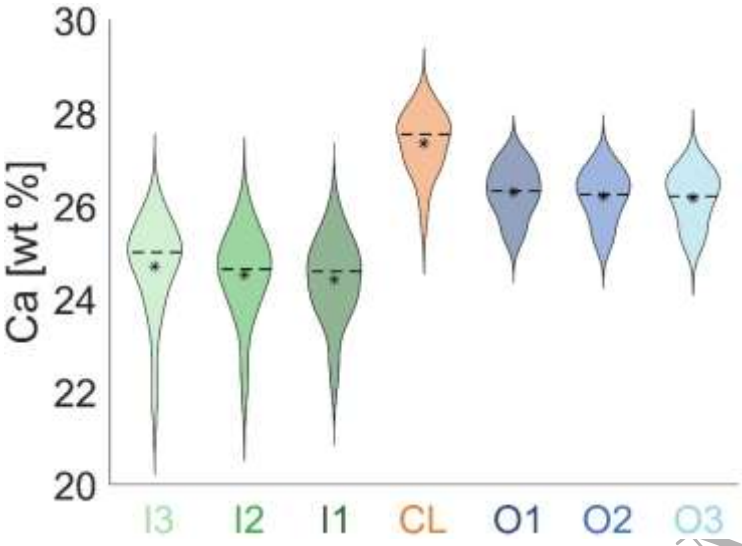

Fig. 4: Violin plots (mirrored histograms) of the calcium content for each segmented region (CL, inner, and outer layers) considering all analyzed osteons (n=35). The mineral content of the CL is significantly higher ($p < 0.001$) than all other layers but O1. The median and mean values are indicated by dashed lines and asterisks, respectively.

The mineralization of the CL is explored in Fig. 5. Firstly, we observed that the mineral content of the CL is always higher than the osteon mineral content, and that a strong correlation is present between them ($R = 0.75$, $p < 0.001$, Fig. 5A), suggesting that the CL mineral content progresses with tissue age. At the same time, the mineral content of the bone outside the osteon (represented by the outer layer O1) had only a moderate correlation ($R = 0.4$, $p = 0.018$) with the mineral content of the osteon (Fig. 5B). In contrast, the relationship between the mineral content of CL and outer layer O1 (Fig. 5C) displays a strong correlation ($R = 0.75$) with statistical significance ($p < 0.001$). As in Fig. 5A, all experimental points are above the line with a slope of 1 (i.e., 45°, dashed lines in Figs. 5A-C). This confirms that the CL is the highest mineralized structure in all 35 investigated osteons compared to either the inside or the outside of the osteon. Virtually identical results are found when considering instead of the outer layer O1, the outer layer O2, which is further away from the CL (Figs. S4A and B). The strong correlation between the mineral content of the CL and the outer layer O1 motivates to investigate how the difference between these two quantities (CL – O1) behaves when plotted versus the osteon mineral content (Fig. 5D). The obtained correlation is strong ($R = 0.75$) and statistically significant ($p < 0.001$). The positive slope of the correlation (full line in Fig. 5D)

shows that the mineral content of the CL deviates more from the mineral content of the surrounding, the older (i.e., the higher mineralized) the osteon is. An opposite trend is observed when plotting (CL – I1) versus the osteon mineral content (Fig. S5).

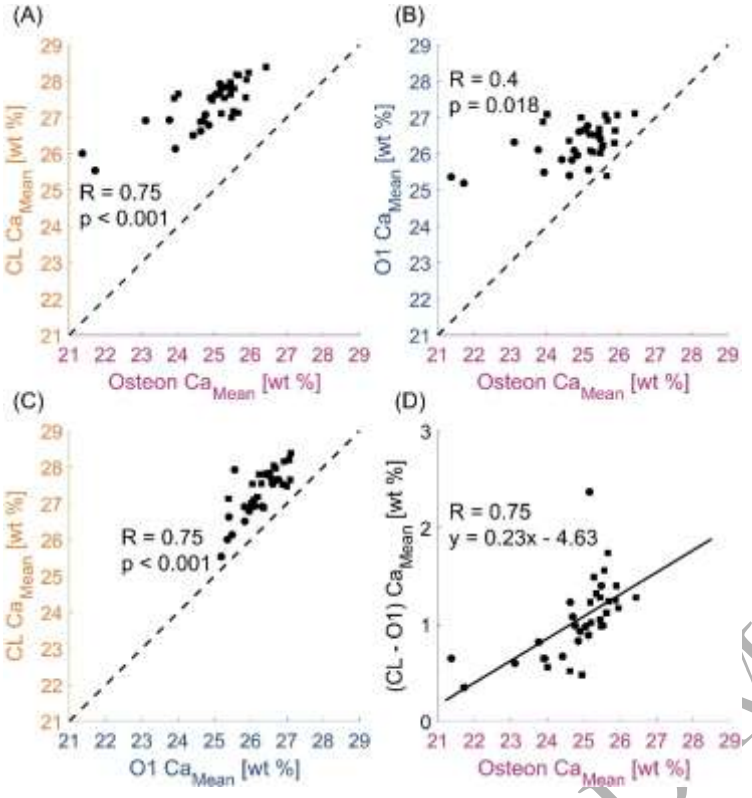

Fig. 5: Relationship between CL, osteon and the outer bone. (A) Correlation between average calcium content (Ca_{Mean}) of the CL and the corresponding osteon, (B) outer layer O1 and osteon, (C) CL and O1, and (D) difference between CL and O1 (CL-O1) and osteon. The dotted line (with a unit slope and passing through the origin) is inserted to improve the readability of the plot. The full line in (D) represents the result of a linear regression. Circles represent osteons from the adult individual (40 years) and square from the aged individual (81 years).

Motivated by the strong correlation between the mineral content of the CL and of the outer layer O1 (Fig. 5C), we performed a spatially resolved analysis of the relationships between the mineralization of the CL and the outer/inner layers, by considering the calcium content within each circular sector around the osteon, for a total of 3920 different regions inspected (Fig. 6). Pooling all sector-wise data together (Fig. S6) confirmed the trend observed in Fig. 5, with CL and O1 showing the highest correlation and data points spread close to a line of unit slope. We applied the sector analysis (presented in Fig. 2F and 3F) to all osteons (Fig. 6A): for 21 out of 35 osteons, we detected a statistically significant correlation ($p < 0.05$) between the mineral content of the CL and outer layer O1, ranging from moderate ($0.4 < R < 0.7$) to strong ($0.7 < R < 0.9$). The osteons which did not show a significant correlation are likely to have higher mineral content ($Ca_{Mean} > 24.6$ wt %). The differences in mineral content between the CL and the closest outer layer (CL - O1) as well as between the CL and the closest inner layer

(CL - I1) were then calculated in each discrete sector and averaged for each osteon (Fig. 6B). The results further underline that the degree of mineralization of the CL is extremely close to the mineral content of the outer layer O1, with the difference CL - O1 being always less than 2 wt % and showing a small increase for more mineralized osteons. In comparison, the differences between CL and I1 are higher (up to 3.5 - 4 wt %) and show a slight decreasing trend with osteon mineral content. A similar behavior is observed when considering all individual sectors (Fig. 6C). Here, we report results as 2D maps with differences (CL - O1) and (CL - I1) calculated in each sector but not averaged in the osteons. In Fig. 6C, the 16 individual sectors are on the vertical axis and the 35 osteons, sorted from lower to higher mineral content, are on the horizontal axis. Results indicate that even in discrete regions around the osteon, the mineral content of the CL is very similar to the degree of mineralization of the outer layer O1; this similarity being particularly strong for osteons with lower mineral content, i.e. assumed to be younger.

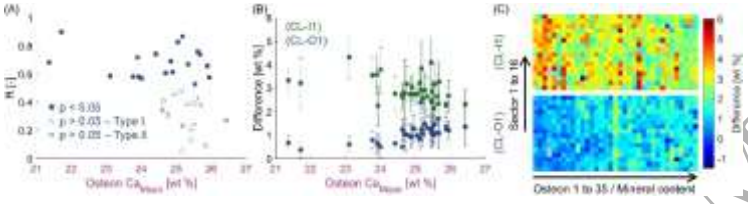

Fig. 6. Spatial analysis of the mineral content. (A) Spearman correlation coefficients between the mineral content of the CL and the outer layer O1. All osteons that show a statistically significant correlation are of type I, whereas among the osteons where no correlation is detected, there are several osteons of type II (i.e., osteon-in-osteon). (B) Differences in mineral content between the CL and the neighboring layers computed as average difference (CL-O1) and (CL-I1) in the circular sectors and plotted versus the mean degree of mineralization of the osteon. Data points represent the mean value and error bars the standard deviation for each osteon. In (A) and (B), circles represent osteons from the adult individual (40 years) and square from the aged individual (81 years). (C) Local differences (CL-O1) and (CL-I1) calculated in each sector (vertical axis) and reported for each osteon sorted according to increasing mineral content (horizontal axis). A few grey pixels indicate sectors where the mineral content could not be calculated, for example due to pores or cracks.

Discussion

In this study we investigated the mineral content of CL and neighboring tissue in cortical bone and we deduced the following aspects of CL mineralization.

The observations that the mineral content of the CL is higher compared to the corresponding osteon and that there is a strong correlation between the mineral content of the CL and of the osteon (Fig. 5A), suggest that the mineral content of the CL also evolves in time. To describe the mineralization process, a separation into a fast primary and a much slower secondary phase is useful. Osteon and CL have a similar tissue age. Nevertheless, the higher mineral content of the CL suggests that in primary mineralization, the CL can incorporate more mineral than the osteon. A previous study on postmenopausal women reported similar trends [16]. However, our work demonstrates that more can be learned when the focus is not restricted to the osteon itself and the outer environment around the CL is explored. Our main finding is that

the mineral content of the CL (after primary mineralization) is closely related to the mineral content of the surrounding in which the CL and the new osteon are formed. This statement is supported by the strong correlation between the average mineral content of the CL and of the external bone (Fig. 5C). Noteworthy, a correlation is even present when considering individual regions around the osteons (Fig. 6), hinting for a local spatial interplay between the older resorbed bone CL and the newly deposited CL. How can such an interplay be explained? A possible explanation should consider the formation of the CL, which takes place on the eroded surface soon after bone resorption and therefore in a local milieu full of mineral ions released by osteoclasts[31][32], with the additional presence of osteopontin, that could further enhance the accumulation of minerals in the newly forming CL[33,34]. It is conceivable that the higher the mineral content of the region undergoing resorption, the more mineral ions are released and used to build the CL. This scenario is compatible with a faster primary mineralization of the CL, explaining also the strong correlation between the mineral content of the CL and of layer O1 (Fig. 5C). As this correlation is higher than the one between osteon and O1 (Fig. 5B), secondary mineralization alone cannot be the only cause for the observed trend. The formation of the bone inside the osteon is somewhat "dephased", both in space (up to 1 mm[1]) and time (up to 50 days, assuming a deposition rate of 20 µm/day[35]), with respect to the deposition of the CL. Thus, the concentration of mineral ions during osteonal bone deposition may be different than during the formation of the CL. This could be one reason of the weak correlation between CLs and bone layers inside the osteon (Fig. S7).

Considering secondary mineralization, figure 5D clearly shows that the difference between the mineral content of the CL and of its outside surrounding increases with tissue age. Since the surrounding of the selected osteons is older bone tissue, which is already in advanced secondary mineralization, it can be assumed that its mineral content hardly changes any more. Consequently, this increasing trend should correspond to the rather slow secondary mineralization of the CL. Based on available data on turnover rate in osteonal bone[36–38], we estimate an age difference of about 15 years between the youngest and the oldest osteon. This means that the mineral content of the CL increases due to secondary mineralization of about 2 wt % over 15 years. In contrast, within the same time span, the increase in osteon mineral content is about 5 wt % (Fig. 5A). A secondary mineralization, which is slower in the CL compared to the osteon, is also consistent with the finding that the higher the mean mineral content of the osteon, the less is the difference in mineralization between the osteon and the CL (Fig. S8).

In some cases the correlation between the mineral content of the CL and the outer surrounding is weak and we could identify a reason for that: many of the osteons with a weak correlation are classified as type II osteons[39–41] also known as "osteon-in-osteon"[42] (Fig. 6A). This term refers to a specific type of relatively large osteon containing a smaller osteon in its center, both

being surrounded by concentric CLs[39,43]. In type II osteons, the degree of mineralization of the external environment around the osteon tends to be more homogenous in comparison to osteons surrounded by both interstitial bone and older osteons (Fig. S9).

In summary, we provide information on the mineralization process of the CL: after primary mineralization, the mineral content of the CL is substantially higher than the mineral content in osteonal bone. Most importantly, the mineral content of the CL after primary mineralization is clearly not universal but depends on the location where the remodeling event occurs, with the CL being more mineralized when the osteon is surrounded by bone of higher mineral content. The CL shows also a secondary mineralization which proceeds at much slower rates than in osteonal bone. One reason for the slower pace may be the high mineral content already attained at the end of primary mineralization. The interplay between primary and secondary mineralization of the CL can be explored with the help of a previously developed mathematical model for the mineralization process of bone[18] (Supplementary Information and Fig. S10): if the CL has an augmented primary mineralization, the secondary mineralization needs to be reduced to avoid attaining unrealistically high values of the mineral content (Fig. S10). The found higher mineral content of all CLs compared to the mineral content of the neighboring osteonal bone agrees with previous works[10,14,16] and one possible explanation is a reduced nanoscale porosity at the CL [25].

The following limitations should be mentioned. A major point concerns the limited sample size of only two male individuals and 35 osteons, mainly because of the time-consuming approach of our analysis. Nonetheless, our observations on the interplay between cement line and osteon mineral content are in full agreement with a prior work[16], corroborating that these findings are not unique to the two individuals studied. Future works should incorporate larger and more diverse samples, coming from individuals of different gender, age as well as considering different anatomical locations. We have selected males for this first investigation to rule out the possible impact on bone mineral content following menopause in women[47]. Another point is about the limited thickness of the CL. We acquired qBEI maps with a resolution of 0.57 µm/pixel and the typical width of the CL in 2D sections is about 1-3 µm. Consequently, there may be a fraction of pixels only partially filled by the CL, leading to partial volume artifacts impacting the detected mineral content. We tried to minimize this issue by considering a 2-pixel layer centered on the CL. While this approach likely underestimates the true thickness of the CL around each osteon in most cases, it provides a conservative estimation of its mineral content. In our work as well as in the literature[16,24,44,45], the osteon mineral content is used as an indicator of tissue age. Although we cannot exclude that mineralization progresses at different speeds in different osteons, the mineral content remains a valuable quantity for studying mineralization in the absence of direct tissue age markers[46]. Although improbable, it

cannot be completely ruled out that freezing and treatment of samples affects the measured mineral content. Nevertheless, all samples were prepared in the identical way, allowing for comparisons between osteons and ensuring validity of found correlations. While this work focuses on mineral content and mineralization, future works should characterize the organic phase for example with Raman microspectroscopy. Such an analysis would give the possibility to detect possible changes in the organic matrix, e.g., the glycosaminoglycan content that might contribute to the observed differences in mineralization.

In conclusion, by taking into consideration the bone outside the osteon, we demonstrate a close spatial interplay between the mineralization of the CL and the mineral content of the surrounding older bone, suggesting that CL mineralization is different in different osteons. Bone diseases or treatments affecting bone mineralization may have a direct impact on the mineral content, and therefore on the mechanical behavior of the CLs.

Conflicts of Interest

The authors declare no competing interests.

Acknowledgements

AC is supported by the French Community of Belgium as part of a FRIA (Fund for Research Training in Industry and Agriculture) grant (n°1E03621F). We warmly thank Phaedra Messmer, Petra Keplinger, and Sonja Lueger from LBIO for the sample preparation. MH and SB gratefully acknowledge financial support from the Austrian Social Health Insurance Fund (OEGK) and the Austrian Workers' Compensation Board (AUVA). MR and RW thank the Max Planck Queensland Centre for the Materials Science of Extracellular Matrices for support.

Data Availability Statement

The datasets generated and analyzed during the current study are available from the corresponding authors on reasonable requests.

Author contributions

Astrid Cantamessa (Conceptualization, Funding acquisition, Data curation, Formal analysis, Investigation, Methodology, Visualization, Writing—original draft, Writing—review & editing), Stéphane Blouin (Conceptualization, Resources, Data curation, Formal analysis, Investigation,

Methodology, Visualization, Writing—original draft, Writing—review & editing), Maximilian Rummler (Data curation, Formal analysis, Methodology, Visualization, Writing—original draft, Writing—review & editing), Andrea Berzlanovich (Resources, Methodology, Writing—review & editing), Richard Weinkamer (Conceptualization, Resources, Data curation, Formal analysis, Investigation, Methodology, Visualization, Supervision, Writing—original draft, Writing—review & editing), Markus A. Hartmann (Conceptualization, Resources, Data curation, Formal analysis, Investigation, Methodology, Visualization, Supervision, Writing—original draft, Writing—review & editing) and Davide Ruffoni (Conceptualization, Funding acquisition, Resources, Data curation, Formal analysis, Investigation, Methodology, Visualization, Supervision, Project administration, Writing—original draft, Writing—review & editing).

References

1. Lassen NE, Andersen TL, Pløen GG, Søe K, Hauge EM, Harving S, Eschen GET, Delaisse J. Coupling of Bone Resorption and Formation in Real Time: New Knowledge Gained From Human Haversian BMUs. J. Bone Miner. Res. 2017 Jul;32(7):1395–405.

2. Lamarche BA, Thomsen JS, Andreasen CM, Lievers WB, Andersen TL. 2D size of trabecular bone structure units (BSU) correlate more strongly with 3D architectural parameters than age in human vertebrae. Bone. 2022 Jul;160:116399.

3. Tits A, Blouin S, Rummler M, Kaux J-F, Drion P, Van Lenthe GH, Weinkamer R, Hartmann MA, Ruffoni D. Structural and functional heterogeneity of mineralized fibrocartilage at the Achilles tendon-bone insertion. Acta Biomater. 2023 Aug;166:409–18.

4. Gupta HS, Schratter S, Tesch W, Roschger P, Berzlanovich A, Schoeberl T, Klaushofer K, Fratzl P. Two different correlations between nanoindentation modulus and mineral content in the bone–cartilage interface. J. Struct. Biol. 2005 Feb;149(2):138–48.

5. Nalla RK, Kruzic JJ, Kinney JH, Ritchie RO. Mechanistic aspects of fracture and R-curve behavior in human cortical bone. Biomaterials. 2005 Jan;26(2):217–31.

6. Koester KJ, Ager JW, Ritchie RO. The true toughness of human cortical bone measured with realistically short cracks. Nat. Mater. 2008 Aug;7(8):672–7.

7. Mohsin S, O'Brien FJ, Lee TC. Osteonal crack barriers in ovine compact bone. J. Anat. 2006 Jan;208(1):81–9.

8. Zimmermann EA, Gludovatz B, Schaible E, Busse B, Ritchie RO. Fracture resistance of human cortical bone across multiple length-scales at physiological strain rates. Biomaterials. 2014 Jul;35(21):5472–81.

9. Wagermaier W, Klaushofer K, Fratzl P. Fragility of Bone Material Controlled by Internal Interfaces. Calcif. Tissue Int. 2015 Sep;97(3):201–12.

10. Gauthier R, Follet H, Olivier C, Mitton D, Peyrin F. 3D analysis of the osteonal and interstitial tissue in human radii cortical bone. Bone. 2019 Oct;127:526–36.

11. Gustafsson A, Wallin M, Khayyeri H, Isaksson H. Crack propagation in cortical bone is affected by the characteristics of the cement line: a parameter study using an XFEM interface damage model. Biomech. Model. Mechanobiol. 2019 Aug;18(4):1247–61.

12. Montalbano T, Feng G. Nanoindentation characterization of the cement lines in ovine and bovine femurs. J. Mater. Res. 2011 Apr 28;26(8):1036–41.

13. Burr DB, Schaffler MB, Frederickson RG. Composition of the cement line and its possible mechanical role as a local interface in human compact bone. J. Biomech. 1988 Jan 1;21(11):939–45.

14. Skedros JG, Holmes JL, Vajda EG, Bloebaum RD. Cement lines of secondary osteons in human bone are not mineral-deficient: New data in a historical perspective. Anat. Rec. A. Discov. Mol. Cell. Evol. Biol. 2005 Sep;286A(1):781–803.

15. Langer M, Pacureanu A, Suhonen H, Grimal Q, Cloetens P, Peyrin F. X-Ray Phase Nanotomography Resolves the 3D Human Bone Ultrastructure. Zuo X-N, editor. PLoS ONE. 2012 Aug 29;7(8):e35691.

16. Milovanovic P, vom Scheidt A, Mletzko K, Sarau G, Püschel K, Djuric M, Amling M, Christiansen S, Busse B. Bone tissue aging affects mineralization of cement lines. Bone. 2018 May;110:187–93.

17. Roschger P, Paschalis EP, Fratzl P, Klaushofer K. Bone mineralization density distribution in health and disease. Bone. 2008 Mar;42(3):456–66.

18. Ruffoni D, Fratzl P, Roschger P, Klaushofer K, Weinkamer R. The bone mineralization density distribution as a fingerprint of the mineralization process. Bone. 2007 May;40(5):1308–19.

19. Bala Y, Farlay D, Delmas PD, Meunier PJ, Boivin G. Time sequence of secondary mineralization and microhardness in cortical and cancellous bone from ewes. Bone. 2010 Apr;46(4):1204–12.

20. Lukas C, Ruffoni D, Lambers FM, Schulte FA, Kuhn G, Kollmannsberger P, Weinkamer R, Müller R. Mineralization kinetics in murine trabecular bone quantified by time-lapsed in vivo micro-computed tomography. Bone. 2013 Sep;56(1):55–60.

21. McKEE MD, Nanci A. Osteopontin and the Bone Remodeling Sequence: Colloidal-Gold Immunocytochemistry of an Interfacial Extracellular Matrix Protein [a]. Ann. N. Y. Acad. Sci. 1995 Aug;760(1):177–89.

22. Everts V, Delaissé JM, Korper W, Jansen DC, Tigchelaar-Gutter W, Saftig P, Beertsen W. The Bone Lining Cell: Its Role in Cleaning Howship's Lacunae and Initiating Bone Formation. J. Bone Miner. Res. 2002 Jan 1;17(1):77–90.

23. McKee MD, Farach-Carson MC, Butler WT, Hauschka PV, Nanci A. Ultrastructural immunolocalization of noncollagenous (osteopontin and osteocalcin) and plasma (albumin and α2HS-glycoprotein) proteins in rat bone. J. Bone Miner. Res. 1993 Apr 1;8(4):485–96.

24. Roschger A, Wagermaier W, Gamsjaeger S, Hassler N, Schmidt I, Blouin S, Berzlanovich A, Gruber GM, Weinkamer R, Roschger P, Paschalis EP, Klaushofer K, Fratzl P. Newly formed and remodeled human bone exhibits differences in the mineralization process. Acta Biomater. 2020 Mar;104:221–30.

25. Tang T, Landis W, Blouin S, Bertinetti L, Hartmann MA, Berzlanovich A, Weinkamer R, Wagermaier W, Fratzl P. Subcanalicular Nanochannel Volume Is Inversely Correlated With Calcium Content in Human Cortical Bone. J. Bone Miner. Res. 2022 Dec 14;jbmr.4753.

26. Roschger P, Fratzl P, Eschberger J, Klaushofer K. Validation of quantitative backscattered electron imaging for the measurement of mineral density distribution in human bone biopsies. Bone. 1998 Oct;23(4):319–26.

27. Roschger P, Eschberger J, Jr HP. Formation of Ultracracks in Methacrylate-Embedded Undecalcified Bone Samples by Exposure to Aqueous Solutions.

28. Lukas C, Kollmannsberger P, Ruffoni D, Roschger P, Fratzl P, Weinkamer R. The Heterogeneous Mineral Content of Bone—Using Stochastic Arguments and Simulations to Overcome Experimental Limitations. J. Stat. Phys. 2011 Jul;144(2):316–31.

29. Hartmann MA, Blouin S, Misof BM, Fratzl-Zelman N, Roschger P, Berzlanovich A, Gruber GM, Brugger PC, Zwerina J, Fratzl P. Quantitative Backscattered Electron Imaging of Bone Using a Thermionic or a Field Emission Electron Source. Calcif. Tissue Int. 2021 Aug;109(2):190–202.

30. Hinkle DE, Wiersma W, Jurs SG. Applied statistics for the behavioral sciences [Internet]. 5th ed. Boston, Mass., [London]: Houghton Mifflin ; [Hi Marketing] (distributor); 2003. Available from: http://catalog.hathitrust.org/api/volumes/oclc/50716608.html

31. Teitelbaum SL. Bone Resorption by Osteoclasts. Science. 2000 Sep;289(5484):1504–8.

32. Vääräniemi J, Halleen JM, Kaarlonen K, Ylipahkala H, Alatalo SL, Andersson G, Kaija H, Vihko P, Väänänen HK. Intracellular Machinery for Matrix Degradation in Bone-Resorbing Osteoclasts. J. Bone Miner. Res. 2004 Sep 1;19(9):1432–40.

33. McKee MD, Nanci A. Osteopontin at mineralized tissue interfaces in bone, teeth, and osseointegrated implants: Ultrastructural distribution and implications for mineralized tissue formation, turnover, and repair. Microsc. Res. Tech. 1996 Feb 1;33(2):141–64.

34. Tang T, Landis W, Raguin E, Werner P, Bertinetti L, Dean M, Wagermaier W, Fratzl P. A 3D Network of Nanochannels for Possible Ion and Molecule Transit in Mineralizing Bone and Cartilage. Adv. NanoBiomed Res. 2022 Apr 28;2100162.

35. Webster J. Integrated Bone Tissue Physiology: Anatomy and Physiology. 2001;

36. Eriksen EF, Melsen F, Sod E, Barton I, Chines A. Effects of long-term risedronate on bone quality and bone turnover in women with postmenopausal osteoporosis. Bone. 2002 Nov;31(5):620–5.

37. Parfitt AM. Misconceptions (2): turnover is always higher in cancellous than in cortical bone. Bone. 2002 Jun;30(6):807–9.

38. Lerebours C, Weinkamer R, Roschger A, Buenzli PR. Mineral density differences between femoral cortical bone and trabecular bone are not explained by turnover rate alone. Bone Rep. 2020 Dec;13:100731.

39. Eriksen M. Histologic estimation of age at death using the anterior cortex of the femur. J. Phys. Anthropol. 1991 Dec;84(2):171–9.

40. Maggiano IS, Maggiano CM, Clement JG, Thomas CDL, Carter Y, Cooper DML. Three-dimensional reconstruction of Haversian systems in human cortical bone using synchrotron radiation-based micro-CT: morphology and quantification of branching and transverse connections across age. J. Anat. 2016 May;228(5):719–32.

41. van Tol AF, Roschger A, Repp F, Chen J, Roschger P, Berzlanovich A, Gruber GM, Fratzl P, Weinkamer R. Network architecture strongly influences the fluid flow pattern through the lacunocanalicular network in human osteons. Biomech. Model. Mechanobiol. 2020 Jun;19(3):823–40.

42. Redelstorff R. Unique bone histology in partial large bone shafts from Aust Cliff (England, Upper Triassic): an early independent experiment in gigantism. Acta Palaeontol. Pol. [Internet]. 2014 [cited 2024 Sep 18]; Available from: http://www.app.pan.pl/article/item/app20120073.html

43. Yoshino M, Imaizumi K, Miyasaka S, Seta S. Histological estimation of age at death using microradiographs of humeral compact bone. Forensic Sci. Int. 1994;64(2):191–8.

44. Gamsjaeger S, Hofstetter B, Zwettler E, Recker R, Gasser JA, Eriksen EF, Klaushofer K, Paschalis EP. Effects of 3 years treatment with once-yearly zoledronic acid on the kinetics of bone matrix maturation in osteoporotic patients. Osteoporos. Int. 2013 Jan;24(1):339–47.

45. Gourion-Arsiquaud S, Burket JC, Havill LM, DiCarlo E, Doty SB, Mendelsohn R, Van Der Meulen MC, Boskey AL. Spatial Variation in Osteonal Bone Properties Relative to Tissue and Animal Age. J. Bone Miner. Res. 2009 Jul 1;24(7):1271–81.

46. Paschalis EP, Betts F, DiCarlo E, Mendelsohn R, Boskey AL. FTIR Microspectroscopic Analysis of Normal Human Cortical and Trabecular Bone. Calcif. Tissue Int. 1997 Dec;61(6):480–6.

47. Farlay D, Bala Y, Rizzo S, Bare S, Lappe JM, Recker R, Boivin G. Bone remodeling and bone matrix quality before and after menopause in healthy women. Bone. 2019 Nov;128:115030.

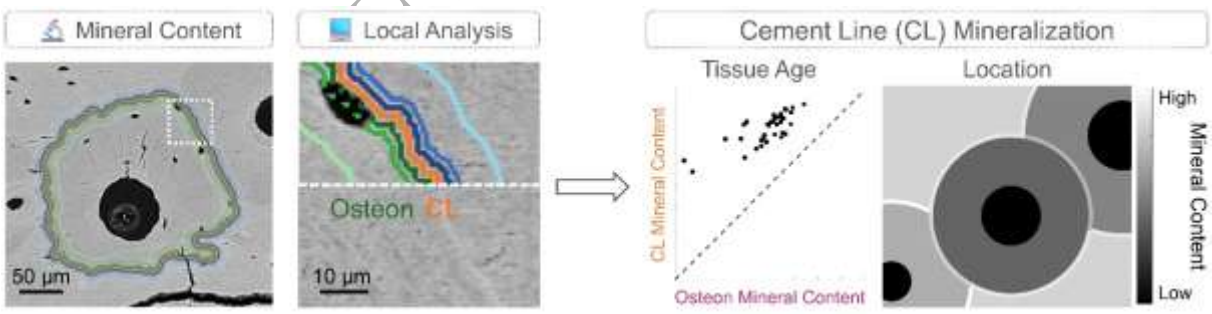

Graphical abstract